

4-8-2021

Periostin loss-of-function protects mice from post-traumatic and age-related osteoarthritis

Mukundan Attur

New York University School of Medicine

Xin Duan

Washington University School of Medicine in St. Louis

Lei Cai

Washington University School of Medicine in St. Louis

Tianzhen Han

New York University School of Medicine

Weili Zhang

Washington University School of Medicine in St. Louis

See next page for additional authors

Follow this and additional works at: https://digitalcommons.wustl.edu/oa_4

Recommended Citation

Attur, Mukundan; Duan, Xin; Cai, Lei; Han, Tianzhen; Zhang, Weili; Tycksen, Eric D; Samuels, Jonathan; Brophy, Robert H; Abramson, Steven B; and Rai, Muhammad Farooq, "Periostin loss-of-function protects mice from post-traumatic and age-related osteoarthritis." *Arthritis research & therapy*. 23, 1. 104 (2021). https://digitalcommons.wustl.edu/oa_4/234

This Open Access Publication is brought to you for free and open access by the Open Access Publications at Digital Commons@Becker. It has been accepted for inclusion in 2020-Current year OA Pubs by an authorized administrator of Digital Commons@Becker. For more information, please contact vanam@wustl.edu.

Authors


Mukundan Attur, Xin Duan, Lei Cai, Tianzhen Han, Weili Zhang, Eric D Tycksen, Jonathan Samuels, Robert H Brophy, Steven B Abramson, and Muhammad Farooq Rai

RESEARCH ARTICLE

Open Access

Periostin loss-of-function protects mice from post-traumatic and age-related osteoarthritis



Mukundan Attur^{1*†}, Xin Duan^{2†}, Lei Cai², Tianzhen Han^{1,3}, Weili Zhang², Eric D. Tycksen⁴, Jonathan Samuels¹, Robert H. Brophy², Steven B. Abramson¹ and Muhammad Farooq Rai^{2,5*} 

Abstract

Background: Elevated levels of periostin (Postn) in the cartilage and bone are associated with osteoarthritis (OA). However, it remains unknown whether Postn loss-of-function can delay or prevent the development of OA. In this study, we sought to better understand the role of Postn in OA development and assessed the functional impact of *Postn* deficiency on post-traumatic and age-related OA in mice.

Methods: The effects of *Postn* deficiency were studied in two murine experimental OA models using *Postn*^{-/-} (*n* = 32) and littermate wild-type (*wt*) mice (*n* = 36). Post-traumatic OA was induced by destabilization of the medial meniscus (DMM) in 10-week-old mice (*n* = 20); age-related OA was analyzed in 24-month-old mice (*n* = 13). Cartilage degeneration was assessed histologically using the OARSI scoring system, and synovitis was evaluated by measuring the synovial lining cell layer and the cells density in the synovial stroma. Bone changes were measured by μ CT analysis. Serum levels of Postn were determined by ELISA. Expression of Postn and collagenase-3 (MMP-13) was measured by immunostaining. RNA-seq was performed on chondrocytes isolated from 21-day old *Postn*^{-/-} (*n* = 3) and *wt* mice (*n* = 3) to discover genes and pathways altered by *Postn* knockout.

Results: *Postn*^{-/-} mice exhibited significantly reduced cartilage degeneration and OARSI score relative to *wt* mice in post-traumatic OA after 8 weeks (maximum: 2.37 ± 0.74 vs. 4.00 ± 1.20 , *P* = 0.011; summed: 9.31 ± 2.52 vs. 21.44 ± 6.01 , *P* = 0.0002) and spontaneous OA (maximum: 1.93 ± 0.45 vs. 3.58 ± 1.16 , *P* = 0.014; summed: 6.14 ± 1.57 vs. 11.50 ± 3.02 , *P* = 0.003). Synovitis was significantly lower in *Postn*^{-/-} mice than *wt* only in the DMM model (1.88 ± 1.01 vs. 3.17 ± 0.63 ; *P* = 0.039). *Postn*^{-/-} mice also showed lower trabecular bone parameters such as BV/TV, vBMD, Tb.Th, and Tb.N and high Tb. Sp in both models. *Postn*^{-/-} mice had negligible levels of serum Postn compared with *wt*. Immunofluorescent studies of cartilage indicated that *Postn*^{-/-} mice expressed lower MMP-13 levels than *wt* mice. RNA-seq revealed that cell-cell-adhesion and cell-differentiation processes were enriched in *Postn*^{-/-} mice, while those related to cell-cycle and DNA-repair were enriched in *wt* mice.

(Continued on next page)

* Correspondence: mukundan.attur@nyulangone.org; rai.m@wustl.edu

[†]Mukundan Attur and Xin Duan contributed equally to this work.

¹Division of Rheumatology, Department of Medicine, New York University Grossman School of Medicine, Langone Orthopedic Hospital, 550 1st Avenue, New York, NY 10016, USA

²Department of Orthopaedic Surgery, Washington University School of Medicine at Barnes-Jewish Hospital MS 8233, 425 South Euclid Avenue, St. Louis, MO 63110, USA

Full list of author information is available at the end of the article



© The Author(s). 2021 **Open Access** This article is licensed under a Creative Commons Attribution 4.0 International License, which permits use, sharing, adaptation, distribution and reproduction in any medium or format, as long as you give appropriate credit to the original author(s) and the source, provide a link to the Creative Commons licence, and indicate if changes were made. The images or other third party material in this article are included in the article's Creative Commons licence, unless indicated otherwise in a credit line to the material. If material is not included in the article's Creative Commons licence and your intended use is not permitted by statutory regulation or exceeds the permitted use, you will need to obtain permission directly from the copyright holder. To view a copy of this licence, visit <http://creativecommons.org/licenses/by/4.0/>. The Creative Commons Public Domain Dedication waiver (<http://creativecommons.org/publicdomain/zero/1.0/>) applies to the data made available in this article, unless otherwise stated in a credit line to the data.

(Continued from previous page)

Conclusions: *Postn* deficiency protects against DMM-induced post-traumatic and age-related spontaneous OA. RNA-seq findings warrant further investigations to better understand the mechanistic role of *Postn* and its potential as a therapeutic target in OA.

Keywords: Periostin, Knee osteoarthritis, Trauma, Aging, MMP-13, RNA-seq

Introduction

Osteoarthritis (OA) is a clinical syndrome that affects more than 50 million people in the USA, with \$185 billion in annual socioeconomic costs [1, 2]. Currently, there are no proven treatments to delay, let alone prevent, the progression of OA. Thus, a treatment that slows or halts disease progression before end-stage joint failure and arthroplasty is sorely needed. OA is recognized as a whole joint disease that affects all tissues (bone, cartilage, synovium, meniscus, and ligaments) [3, 4], although cartilage degeneration is considered the hallmark of end-stage disease [5]. Despite advances in preclinical studies, the pathways controlling early cartilage degeneration and new bone formation in OA remain unknown. Therefore, a critical issue in OA treatment is discovering early OA mediators, particularly elucidating the underlying intracellular signal transduction pathways, which affects multiple tissues in the joints.

Emerging evidence indicates periostin (*Postn*) is up-regulated in patients with OA [6–9] and has been identified as a gene of interest in articular cartilage [10–12]. *Postn* is a vitamin K-dependent and glutamate-containing matricellular protein [13]. *Postn*, a member of the fasciclin family of proteins, was originally called osteoblast-specific factor 2 [14]. First identified in murine osteoblasts, it is also found in the periosteum [15]. *Postn* plays key roles in health and disease across various disciplines such as osteology and oncology [16–20]. It also plays a role in the repair mechanism of many connective tissues and organs such as the periodontal tissue, heart, and lungs [15, 16, 20–23]. *Postn* is considered important for its role in maintaining tissue integrity. In the bone, *Postn* is predominantly expressed in the periosteum and considered a key extracellular matrix (ECM) protein needed in health and healing. For instance, loss of *Postn* influences the propensity to fatigue fractures in mice [24], and *Postn*-deficient periosteum cannot reconstitute stem cells after injury [25]. Despite this evidence for the importance of *Postn*, it also has an adverse role in various inflammatory settings [26–28].

We have shown that expression of *Postn* is induced following joint trauma such as destabilization of the medial meniscus (DMM) or anterior cruciate ligament transection/partial medial meniscectomy and leads to development and progression of OA [12, 22]. Recently, our data confirmed that the *Postn* expression increases

significantly in mouse and human cartilage and osteophytes during OA progression. Immune-localization studies further revealed that *Postn* was present in the cartilage ECM [10, 12, 22]. Emerging evidence supports the involvement of *Postn* in Wnt signaling activation and MMP-13 expression. *Postn*-induced MMP-13 expression was also inhibited by CCT031374 hydrobromide, an inhibitor of the canonical Wnt/ β -catenin signaling pathway [12]. These findings suggest a catabolic role for *Postn* in promoting cartilage degeneration in OA by upregulating MMP-13 in response to injury.

In the present study, we hypothesize that genetic *Postn* loss-of-function in mice would protect against cartilage degeneration, synovitis, and bone changes secondary to aging and knee injury. To test this hypothesis, we assessed cartilage degeneration, synovial pathology, and bone morphometric parameters in two animal models. One consisting of 24-month-old mice with spontaneous OA and one with surgically induced OA model in 10-week-old mice. *Postn* knockout mice were compared to wild-type (*wt*) in both cohorts. We also performed RNA-seq on chondrocytes isolated from both *Postn*^{-/-} and *wt* mice in a pursuit to identify genes and pathways altered following *Postn* knockout.

Methods

Animals

In this study, we used homozygous mutant *Postn*^{tm1Jmol/J} (*Postn*^{-/-}; Stock No. 009067) mice on a B6129SF2/J (*wt*; Stock No. 101045) background. *Postn*^{-/-} and *wt* mice were obtained from The Jackson Laboratories (Bar Harbor, ME). Post-traumatic OA studies were performed at Washington University (St. Louis, MO), and aging studies were conducted at New York University Grossman School of Medicine (New York, NY). *Postn*^{-/-} mice were obtained by crossing heterozygous mice, and littermate mice from the same breeding were used for all experiments. All mice were kept and bred at the study institutions and genotyped by polymerase chain reaction (PCR) using tail deoxyribonucleic acid separated on 1.5% agarose gel using standard methods. Mice were housed in individually ventilated cages, with each cage having no more than five mice at a time in a hygienic barrier facility operating at 21–22 °C. Food and water were available *ad libitum*, and animals were maintained in a 12-h light, 12-h dark cycle. We used only male mice given sex

differences in the DMM model [29]. The number of mice in each experimental group and each genotype are indicated in figure legends and summarized in Table 1.

Detection of Postn protein in the murine serum

Postn deficiency in *Postn*^{-/-} mice was detected by solid-phase enzyme-linked immunosorbent assay (ELISA). Briefly, mice euthanized by carbon dioxide asphyxiation were exsanguinated by cardiac puncture using mini-collect serum separator tubes (Greiner Bio-One, Monroe, NC). The blood was allowed to clot at room temperature for 30 min and retract at 4 °C for 4 h. The clotted blood was centrifuged at 2500 rpm at 4 °C for 10 min. The serum was collected, centrifuged, and stored at -20 °C until used. Postn concentration in serum was measured using a mouse periostin/OSF-2 Quantikine ELISA kit according to the manufacturer's instructions (MOSF20, R&D Systems Inc., Minneapolis, MN). In brief, 50 µl assay diluent was added to each well of a 96-well strip plate followed by an equal volume of standard, control, and sample in individual wells. The plate was incubated at room temperature on a horizontal orbital microplate shaker. After 2 h of incubation, the contents were removed, and each well was washed five times with the supplied wash buffer. Subsequently, 100 µl conjugate was added to each well followed by 2-h incubation at room temperature with constant shaking. Then, following washing as above, the plate was incubated with 100 µl substrate solution in each well for 30 min. Finally, the reaction was terminated with the addition of 100 µl of stop solution and the plate was read at 450 nm within 30 min.

Induction of post-traumatic OA

To determine the role of Postn loss-of-function in post-traumatic OA, we performed the DMM surgery on 10-week-old male *Postn*^{-/-} or *wt* mice as described [30]. In short, mice were anesthetized with 2.5% isoflurane in 4 L/min oxygen. After aseptic preparation of the right

hind limb, the joint capsule immediately medial to the patellar tendon was cut open, and the anterior attachment of the medial meniscotibial ligament was severed with sterilized microsurgical tools. This step resulted in the destabilization of the medial meniscus. Afterward, the joint capsule was closed with 6-0 absorbable polypropylene sutures (Ethicon, Blue Ash, OH), and the skin was closed by Vetclose skin glue (Henry Schein, Melville, NY). However, we used the contralateral left hind limb as non-operated control to avoid the effect of surgery. In compliance with guidelines, sustained-release buprenorphine (1.0 mg/kg) was administered once as an analgesic before surgery. No other pain-relieving medication was given to the mice. All mice were weight-bearing following recovery from the general anesthesia and resumed previous cage activity, water consumption, and food intake. Mice were euthanized 8 weeks after surgery by carbon dioxide inhalation. Hind limbs were separated, skinned, and subjected to histological and micro-computed tomography (µCT) analyses.

Age associated spontaneous OA

For aging studies, 24-month-old *wt* and *Postn*^{-/-} mice were sacrificed using carbon dioxide asphyxiation; the hind limbs were separated, skinned, and prepared for histological and µCT analyses.

Histological assessment of cartilage degeneration and OA

The knee joints were fixed in 10% neutral-buffered formalin for 48 h and decalcified using 12% formic acid, then embedded in paraffin using standard methods. Twelve coronal sections, each with 5 µm thickness, were taken from each joint at eight levels separated by 80 µm intervals. From each level, three sections were stained with Safranin O [31]. In each genotype, the same number and depth of sections were evaluated. The semi-quantitative Osteoarthritis Research Society International (OARSI) scoring system (scale: 0–6) was used to assess cartilage damage [32]. Cartilage damage was measured and scored in all four tibiofemoral compartments of the knee (lateral and medial femoral condyles and lateral and medial tibial plateaus) at all sectioned levels. The maximum OARSI score representing the highest score within all sectioned levels of the knee was recorded. Summed OARSI score was calculated by adding the total scores of four consecutive levels of each knee. Two independent scorers blinded to genotype and procedure scored the sections with a high inter-rater reliability.

Histological assessment of synovitis

Safranin O-stained sections were graded for synovitis in the medial compartment for two parameters using a method developed by Lewis and colleagues [33].

Table 1 Distribution of mice for each experiment

Genotype	Age	Experiment	n
<i>Postn</i> ^{-/-}	10 weeks	DMM	10
	24 months	Aging	7
	24 months	Serum	6
	21 days	RNA-seq	3
	21 days	Real-time PCR	6
<i>wt</i>	10 weeks	DMM	10
	24 months	Aging	6
	24 months	Serum	11
	21 days	RNA-seq	3
	21 days	Real-time PCR	6

Enlargement of the synovial lining cell layer is measured on a scale of 0–3, separately from the cells' density in the synovial stroma on a scale of 0–3. Synovitis scores obtained for both of these parameters were averaged separately, and the sum of averages from both parameters used for analysis on a scale of 0–6.

Immunostaining for Postn and MMP-13

Histological sections were deparaffinized using xylene and then rehydrated in a graded series of ethyl alcohol. Endogenous peroxidase activity quenched by incubating slides with 3% (v/v) hydrogen peroxide in phosphate-buffered saline (PBS). After 15 min of incubation, proteinase K (10 µg/mL, Abcam, Cambridge, MA) was added to the sections for 20 min at 37 °C to retrieve the antigen. Following washing with PBS and blocking with 10% normal goat serum (NGS), slides were allowed to react overnight at 4 °C with the following primary antibodies diluted in 2% NGS: anti-periostin (1:100, Sigma-Aldrich, St. Louis, MO), MMP-13 (1:200, Abcam), and in-house collagen type II (Col 2, 1:200). The next day, following the washing step, slides were incubated with the corresponding HRP- (for Postn), Alexa 488-(MMP-13), or Alexa 594-(for Col 2) conjugated secondary antibody in 2% NGS for one-hour room temperature. Then, slides (MMP-13 and Col 2) underwent counterstaining with Fluoro-Gel II with 4',6-diamidino-2-phenylindole (DAPI, Electron Microscopy Sciences, Hatfield, PA) for MMP-13 and Col 2. For immunohistochemical staining of Postn, HRP stained slides were developed with 3,3'-Diaminobenzidine (DAB Chromogen Kit; Vector Laboratories Inc., Burlingame, CA) for 10 min at room temperature. All images were visualized using a NanoZoomer (Hamamatsu Corp., Bridgewater, NJ) or Confocal Laser Scanning Microscope (Leica, Biosystems, Buffalo Grove, IL). MMP-13 expression levels were quantified by measuring the staining intensity of 20–40 cells in each stained section using LAS X software (Leica Biosystems).

µCT analysis of the trabecular bone

After fixation but before decalcification, the knees undergoing DMM were scanned using a vivaCT 40 in vivo µCT scanner (Scanco Medical Inc., Southeastern, PA) with the following setting: voxel size = 21 µm, energy = 45 kV, intensity = 177 µA, and integration time = 300 ms [34]. To analyze bone changes, the femoral epiphysis was chosen as the region of interest. The region of interest was identified between the cartilage and the growth plate. The outline of the epiphysis was carefully selected without the inclusion of outgrowing osteophyte(s). Knees from 24-month-old mice were scanned using a 10 MP digital detector using the following parameters: 10 W of energy (50 kV and 200 mA), pixel size = 9.7 µm, exposure = 1025 ms/frame, rotation step 0.3 degrees with × 10 frames averaging, 0.5 mm Aluminum filter, and scan rotation = 180°. After scanning, the

radiographs were reconstructed using NRecon software ver. 1.7.3.0 (Bruker µCT, Kontich, Belgium). Reconstruction was done with NRecon using GPU acceleration. Gaussian smoothing was applied with a 2-voxel radius, ring artifact, and beam hardening corrections were applied in reconstruction. Ring artifact reduction set to 7 pixels. Beam hardening correction was set to 40%. Following trabecular bone morphometric parameters defined by the American Society for Bone and Mineral Research were analyzed [35]: bone volume fraction (BV/TV), volumetric bone mineral density (vBMD), trabecular thickness (Tb.Th), trabecular number (Tb.N), and trabecular spacing (Tb.Sp).

RNA-Seq analysis, gene ontology annotation, and transcript expression validation

We performed bulk RNA-seq on articular chondrocytes isolated from *Postn*^{-/-} and *wt* mice to determine the baseline transcript-level differences between the two genotypes.

Chondrocyte isolation and culture

Primary chondrocytes were isolated from femoral head cartilage of 21-day-old *Postn*^{-/-} (*n* = 3) and *wt* (*n* = 3) mice as described previously [36]. The cells were seeded in 24-well plates, supplied with 10% fetal bovine serum (FBS; Thermo Fisher Scientific, Waltham, MA) in high glucose Dulbecco's modified Eagle's medium (DMEM; Thermo Fisher Scientific) supplemented with 1% penicillin and streptomycin (10,000 U/mL and 10,000 µg/mL respectively; Thermo Fisher Scientific) and incubated at 37 °C in a humidified incubator with 5% CO₂. After 2 days of culture, cells were washed 3× with PBS before RNA extraction.

RNA extraction

Total RNA was extracted from 1.0 × 10⁵ cells using a column-based RNeasy Mini kit (Qiagen, Valencia, CA). Total RNA quality and concentrations were measured using Agilent Bioanalyzer (Agilent Technologies Inc., Santa Clara, CA). RNA samples with a RIN (RNA integrity number) score > 9.0 were used for RNA-seq analysis and real-time PCR.

Library preparation, sequencing, and gene ontology analysis

Library preparation was performed with 10 ng of total RNA. Double-stranded cDNA was prepared using Clontech SMARTer Ultra Low RNA kit (Takara Bio Inc., Mountain View, CA). cDNA was fragmented with an E220 sonicator (Covaris Inc., Woburn, MA) using these settings: peak incident power = 18, duty factor = 20%, and cycles per burst = 50 for 120 s. cDNA was blunt-ended, had an A base added to the 3' ends, and had Illumina sequencing adapters ligated to the ends. Ligated fragments were amplified for 12–15 cycles using primers incorporating unique dual index tags. Fragments were sequenced on an Illumina HiSeq 3000 (Illumina, San

Diego, CA) using single-end reads extending 50 bases. Base calls and demultiplexing performed with Illumina's bcl2fastq software, and a custom python demultiplexing program with a maximum of one mismatch in the indexing read. RNA-seq reads were aligned to the Ensembl release 76 top-level assemblies with STAR version 2.0.4b [37]. Gene counts were derived from the number of uniquely aligned unambiguous reads by Subread:featureCount version 1.4.5 [38]. Sequencing performance was assessed for the total number of aligned reads, the total number of uniquely aligned reads, and features detected. The ribosomal fraction, known junction saturation, and read distribution over known gene models were quantified with RSeQC version 2.3 [39].

All gene counts imported into the R/Bioconductor package EdgeR [40], and TMM normalization size factors were calculated to adjust for samples for differences in library size. Ribosomal genes and genes not expressed in the smallest group size minus one sample greater than one count-per-million excluded from further analysis. The TMM size factors and the matrix of counts were then imported into the R/Bioconductor package Limma [41]. Weighted likelihoods based on the observed mean-variance relationship of every gene and sample were then calculated for all samples with the voomWithQualityWeights [42] function with additional unknown latent effects as determined by surrogate variable analysis [43]. All genes performance assessed with plots of the residual standard deviation of every gene to their average log-count with a robustly fitted trend line of the residuals. Differential expression analysis was performed to analyze for differences between conditions, and the results were filtered for only those genes with Benjamini-Hochberg false-discovery rate (FDR) adjusted $P \leq 0.05$.

For each contrast extracted with Limma, global perturbations in known Gene Ontology (GO) terms detected using the R/Bioconductor package "Generally Applicable Gene set Enrichment" [44] to test for changes in expression of the reported \log_2 -fold changes reported by Limma in each term versus the background \log_2 -fold of all genes found outside the respective term. The R/Bioconductor package heatmap3 [45] used to display heatmaps across groups of samples for each GO term with a Benjamini-Hochberg FDR-adjusted $P \leq 0.05$.

Validation of RNA-seq data by quantitative real-time PCR

We validated RNA-seq data by quantitative real-time PCR. We selected representative genes for each pattern of expression. Expression of *Dscaml1* and *Tm4sf1* was higher in *Postn*^{-/-} and *wt* mice respectively, expression of *Ndufs5* and *Srsf10* was similar in both groups. Total RNA was prepared from chondrocytes isolated from *Postn*^{-/-} mice ($n = 6$) and *wt* mice ($n = 6$) mice. A total of 250 ng of total RNA was subjected to Amplification Grade

DNase I treatment (1 U/ μ L, Thermo Fisher Scientific), to eliminate traces of genomic DNA and then reverse transcribed to synthesize the first strand of cDNA (High-Capacity Reverse Transcription Kit, Thermo Fisher Scientific). Briefly, 2 μ L cDNA was added to the reaction mixture comprising of 2 \times SYBR Green Master Mix (Thermo Fisher Scientific), gene-specific forward and reverse primers (primer sequences are depicted in Table 2), and RNase-free water to reach a total volume of 20 μ L. Subsequently, real-time PCR was performed under the following settings: 94 °C for 3 min, followed by 40 cycles at 94 °C for 30 s, 60 °C for 30 s, and 72 °C for 30 s. The target gene expression was normalized to the housekeeping gene, *Gapdh*. Each analysis was performed in triplicate. The relative expression values were computed using $2^{-\Delta\Delta Ct}$ method.

Statistical analysis

The non-parametric Mann-Whitney test used to compare the data from two genotypes (*wt* and *Postn*^{-/-}) unless indicated otherwise. Results were considered statistically significant at $P < 0.05$. Data are presented as mean \pm standard deviation with 95% confidence interval (CI) where indicated. All statistical analyses were performed using GraphPad PRISM version 7.03 (GraphPad Software Inc., San Diego, CA).

Results

Postn^{-/-} mice exhibit no Postn in the joint and in the serum

The genotype of each mouse was confirmed by PCR (Fig. 1a–c). We demonstrated a complete loss of Postn protein in *Postn*^{-/-} mice by immunostaining of the joint section (Fig. 1d) and ELISA in serum. ELISA results revealed significantly low levels of Postn protein in the serum of *Postn*^{-/-} mice compared with the *wt* mice (28.33 ± 21.65 [95% CI = -4.88–61.55] vs. 3827.00 ± 2504.00 [95% CI = 2144.00–5509.00], $P = 0.0002$) (Fig. 1e).

Postn^{-/-} mice develop less severe OA after DMM Cartilage degeneration

The analysis of histological sections of DMM-operated or non-operated knees from *Postn*^{-/-} and *wt* mice at 8-weeks after DMM surgery (Fig. 2a) showed that non-operated control mice retained relatively normal cartilage with maximum OARSI score ≤ 1.00 . Conversely, many histological features representative of OA were apparent 8 weeks after surgery in *wt* mice: reduced Safranin O staining depicting proteoglycan loss in the ECM, fibrillation, and delamination of superficial zone cartilage, and in severe cases, an extension of the cleft lesions into the middle zone. These features illustrate that DMM surgery-induced degeneration of the cartilage resembles human OA pathology. The mean maximum OARSI score for *wt* mice in DMM-operated knees

Table 2 Sequence and characteristics of primers used for real-time PCR

Gene symbol	Forward primer (5' → 3')	Location	Reverse primer (5' → 3')	Location	Amplicon size	Accession no.
<i>Dscaml1</i>	aggctgaagaggctacgaga	4972–4991	gaggtcctttcacaggggtg	5062–5043	91 bp	NM_001081270.2
<i>Tm4sf1</i>	actgggtttggcagaaggac	1006–1025	tgggctcatagcacttgac	1127–1108	122 bp	NM_008536.4
<i>Ndufs5</i>	acagccataagaacgccg	148–167	tgtaccgaagcaagcactct	287–268	140 bp	NM_001030274.1
<i>Srsf10</i>	acgtcggaatttggtcggt	234–253	agcgtcttcagatcacgaa	357–338	124 bp	NM_010178.3
<i>Gapdh</i>	aggtcggtgtgaacggattg	100–120	tgtagaccatgtagttgaggtca	222–200	123 bp	NM_001289726.1

bp = base pair

(4.00 ± 1.20 ; 95% CI = 3.00–5.00) was significantly ($P < 0.001$) higher than that of non-operated control knees (0.75 ± 0.46 ; 95% CI = 0.36–1.14). *Postn*^{-/-} mice that underwent DMM showed significantly less cartilage damage with the mean maximum OARSI score of 2.37 ± 0.74 (95% CI = 1.75–3.00), significantly ($P = 0.011$) lower than for their littermate *wt* mice (4.00 ± 1.20 ; 95% CI = 3.00–5.00) (Fig. 2b). Likewise, DMM-operated *Postn*^{-/-} mice (9.31 ± 2.52 , 95% CI = 7.21–11.42) had significantly ($P = 0.0002$) lower mean summed OARSI score than *wt* mice (21.44 ± 6.01 , 95% CI = 16.41–26.46) (Fig. 2c).

Synovitis

We noted a thinner synovial lining cell layer and a low density of cells in the synovial stroma in *Postn*^{-/-} mice than *wt* mice (Fig. 2d). Quantification of synovitis score was significantly ($P = 0.039$) lower in *Postn*^{-/-} mice

(1.88 ± 1.01 ; 95% CI = 0.82–2.93) than *wt* mice (3.17 ± 0.63 ; 95% CI = 2.51–3.82) (Fig. 2e).

Trabecular bone changes

Interestingly, there were no differences in the bone parameters measured in the control/contralateral limbs between the genotypes (Table 3). The differences in the various parameters of trabecular bone between *wt* and *Postn*^{-/-} are shown in Fig. 2f. We noted that the following bone parameters were significantly lower in *Postn*^{-/-} mice compared with *wt* mice: trabecular BV/TV (9.8%, $P = 0.009$), vBMD (11.3%, $P = 0.029$), Tb.Th (25.6%, $P = 0.043$), and Tb.N (14.6%, $P = 0.012$). In contrast, Tb. Sp was significantly higher in *Postn*^{-/-} mice than *wt* mice (17.2%, $P = 0.023$).

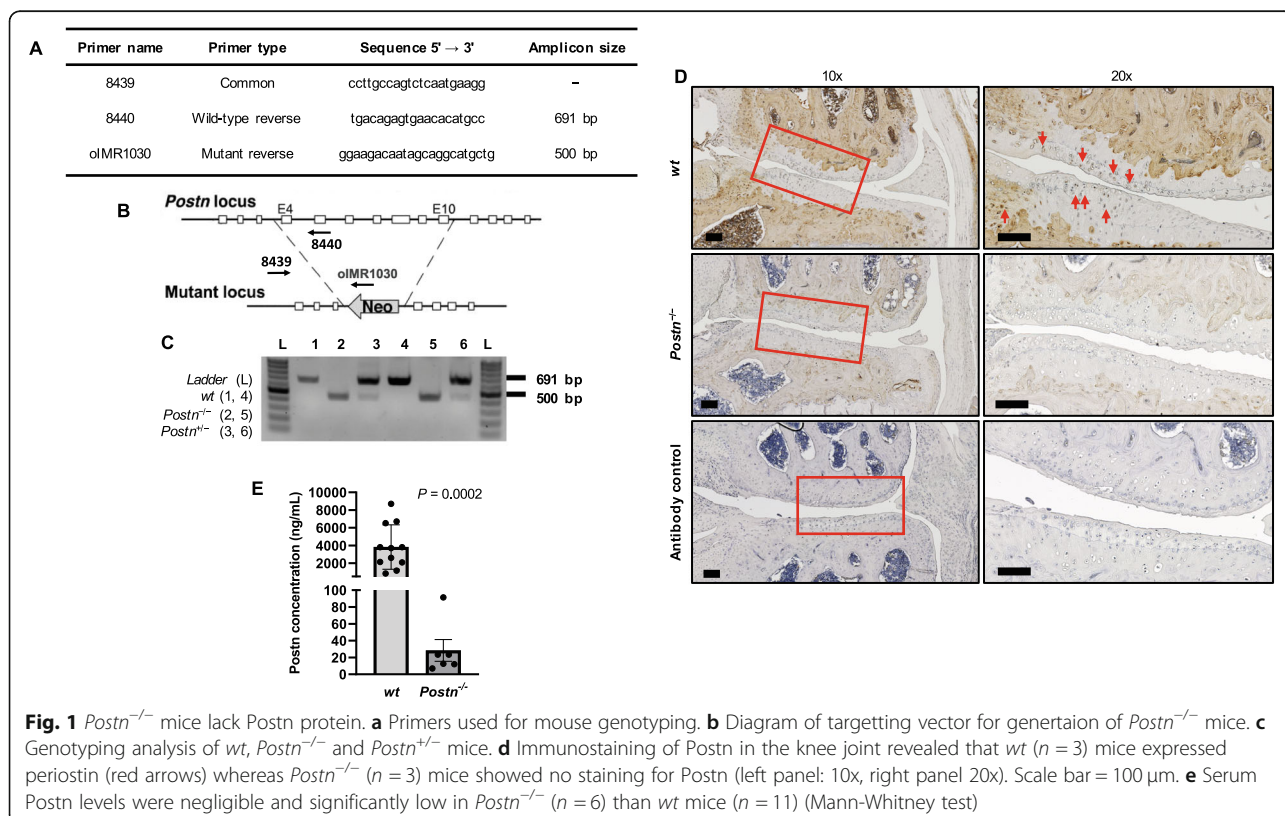
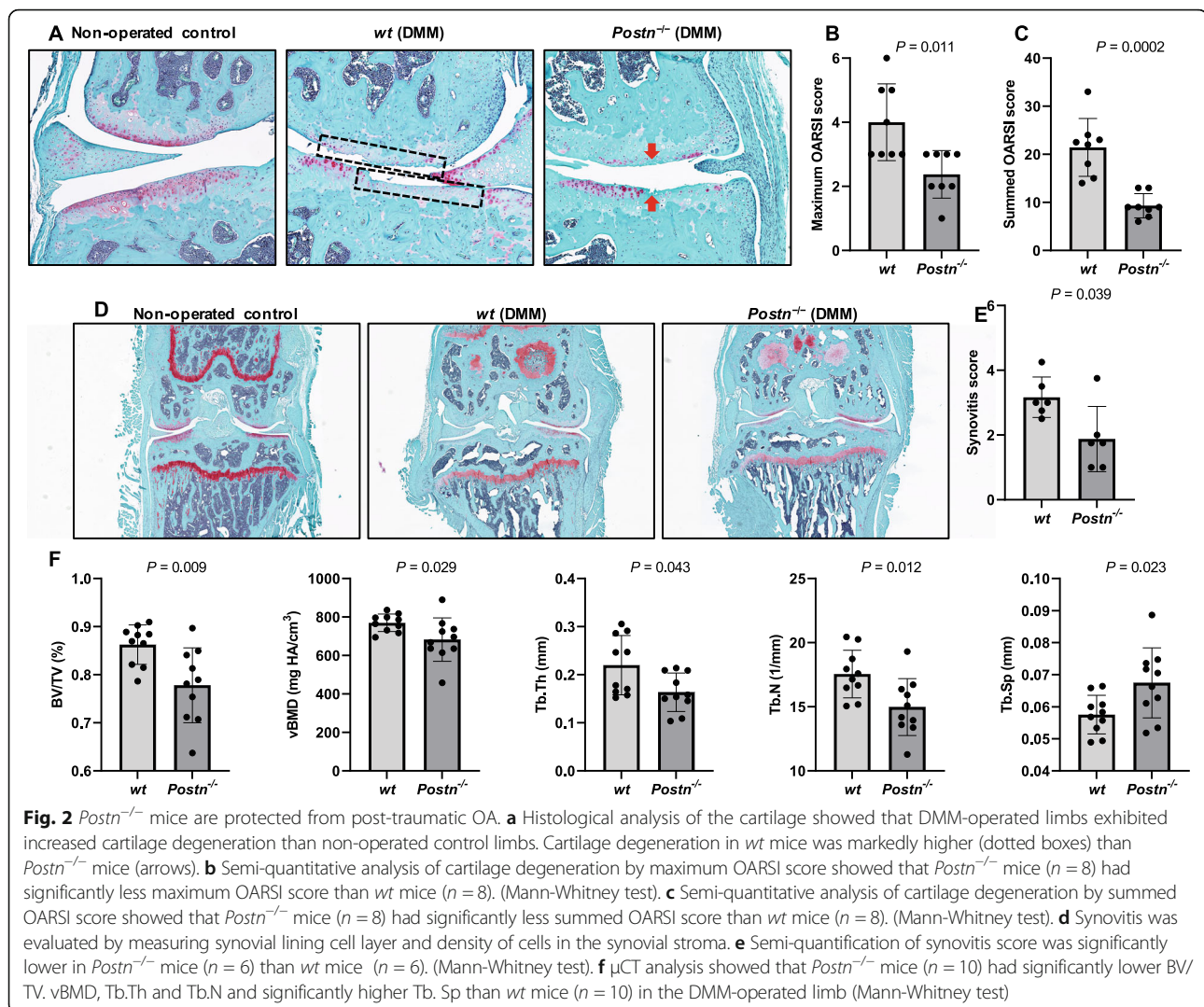


Fig. 1 *Postn*^{-/-} mice lack Postn protein. **a** Primers used for mouse genotyping. **b** Diagram of targeting vector for generation of *Postn*^{-/-} mice. **c** Genotyping analysis of *wt*, *Postn*^{-/-} and *Postn*^{+/-} mice. **d** Immunostaining of Postn in the knee joint revealed that *wt* ($n = 3$) mice expressed periostin (red arrows) whereas *Postn*^{-/-} ($n = 3$) mice showed no staining for Postn (left panel: 10x, right panel 20x). Scale bar = 100 μ m. **e** Serum Postn levels were negligible and significantly low in *Postn*^{-/-} ($n = 6$) than *wt* mice ($n = 11$) (Mann-Whitney test)



24-month-old *Postn*^{-/-} mice demonstrated protection from spontaneous OA

Cartilage degeneration

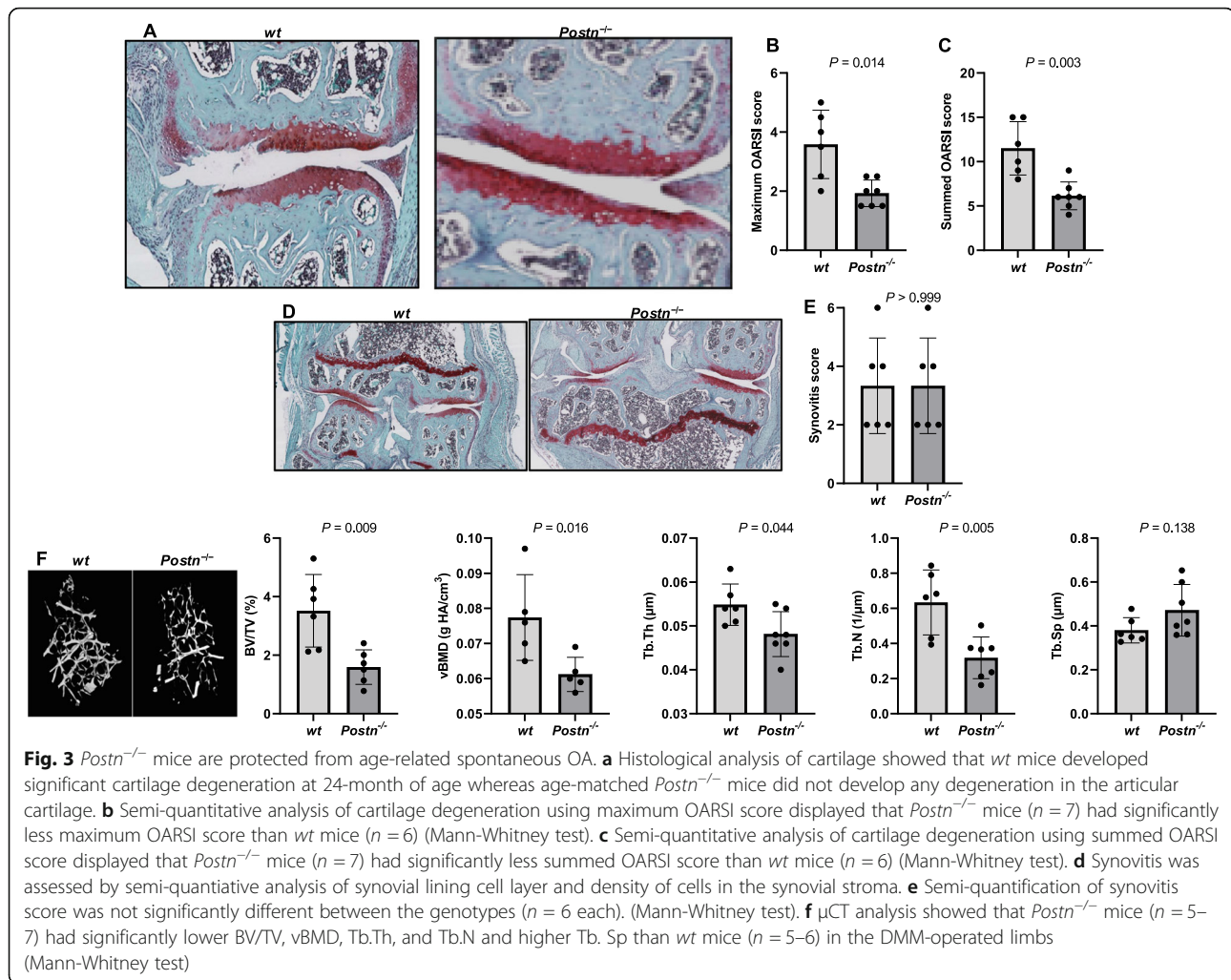
Representative histological sections from 24-month-old *Postn*^{-/-} and *wt* mice are shown in Fig. 3a. Histological analysis of the knee joints of 24-month-old *Postn*^{-/-} and *wt* mice showed that *Postn*^{-/-} mice had less cartilage degeneration (only focal loss of proteoglycans without

cartilage loss) than *wt* mice, which exhibited increased loss of cartilage proteoglycan and delamination of both superficial and middle zones. These observations confirmed that in mice, aging induces spontaneous cartilage degeneration that resembles OA pathology in humans. The mean maximum OARSI score in *Postn*^{-/-} mice was significantly lower than in *wt* mice (1.93 ± 0.45 [95% CI = 1.51–2.35] vs. 3.58 ± 1.16 , [95% CI = 2.37–4.80], *P* =

Table 3 Bone epiphyseal parameters in control limbs of *wt* and *Postn*^{-/-} mice

Parameter	<i>wt</i>		<i>Postn</i> ^{-/-}		<i>P</i> value
	Mean \pm SD	95% CI	Mean \pm SD	95% CI	
BV/TV (mm ³ /mm ³)	0.79 \pm 0.04	0.76–0.82	0.73 \pm 0.09	0.66–0.79	0.143
vBMD (mg HA/cm ³)	650.70 \pm 57.35	609.70–691.70	608.90 \pm 103.60	534.70–682.90	0.436
Tb.Th (mm)	0.20 \pm 0.11	0.13–0.28	0.15 \pm 0.03	0.13–0.17	0.248
Tb.N (1/mm)	14.46 \pm 2.54	12.64–16.28	15.33 \pm 2.87	13.28–17.39	0.631
Tb.Sp (mm)	0.07 \pm 0.02	0.06–0.08	0.06 \pm 0.01	0.05–0.07	0.353

SD standard deviation, CI confidence interval



0.014) (Fig. 3b). Similarly, the mean summed OARSI score was significant ($P = 0.003$) lower in *Postn*^{-/-} mice (6.14 ± 1.57 , 95% CI = 4.69–7.60) than *wt* mice (11.50 ± 3.02 , 95% CI = 8.33–14.67) (Fig. 3c).

Synovitis

The synovial lining cell layer and cell density in the synovial stroma appeared similar in both genotypes (Fig. 3d). We did not find any significant ($P > 0.999$) difference in synovitis score between *Postn*^{-/-} mice (3.33 ± 1.63 ; 95% CI = 1.62–5.05) and *wt* mice (3.33 ± 1.63 ; 95% CI = 1.62–5.05) (Fig. 3e).

Trabecular bone changes

The changes in different trabecular bone parameters are depicted in Fig. 3f. We observed that *Postn*^{-/-} mice exhibited significantly lower trabecular BV/TV (54.7%, $P = 0.009$), vBMD (20.9%, $P = 0.016$), Tb.Th (12.2%, $P = 0.044$) and Tb.N (49.7%, $P = 0.005$) in contrast to *wt*

mice. Also, Tb. Sp was 24.0% higher in *Postn*^{-/-} than *wt* mice but did not reach significance ($P = 0.138$).

MMP-13 expression decreased in *Postn*^{-/-} mice

Immuno-fluorescence analysis of MMP-13 revealed that its expression was increased in *wt* mice following DMM compared with the control knees. In contrast, no MMP-13 was detected in DMM-operated knees of *Postn*^{-/-} mice (Fig. 4a). Semi-quantitative assessment of immuno-fluorescence imaging further showed that intensity of MMP-13 staining was significantly ($P = 0.029$) lower in *Postn*^{-/-} (6.73 ± 5.23 , 95% CI = -1.60–15.06) than *wt* mice (28.18 ± 14.94 , 95% CI = 4.42–51.95) (Fig. 4b).

RNA-seq and gene ontology analyses

Qualitative gene expression analysis revealed that samples were clustered into two distinct clusters of *Postn*^{-/-} and *wt* chondrocytes based on principal component analysis indicating a specific expression profile (Fig. 5a) though there was higher variation among samples from

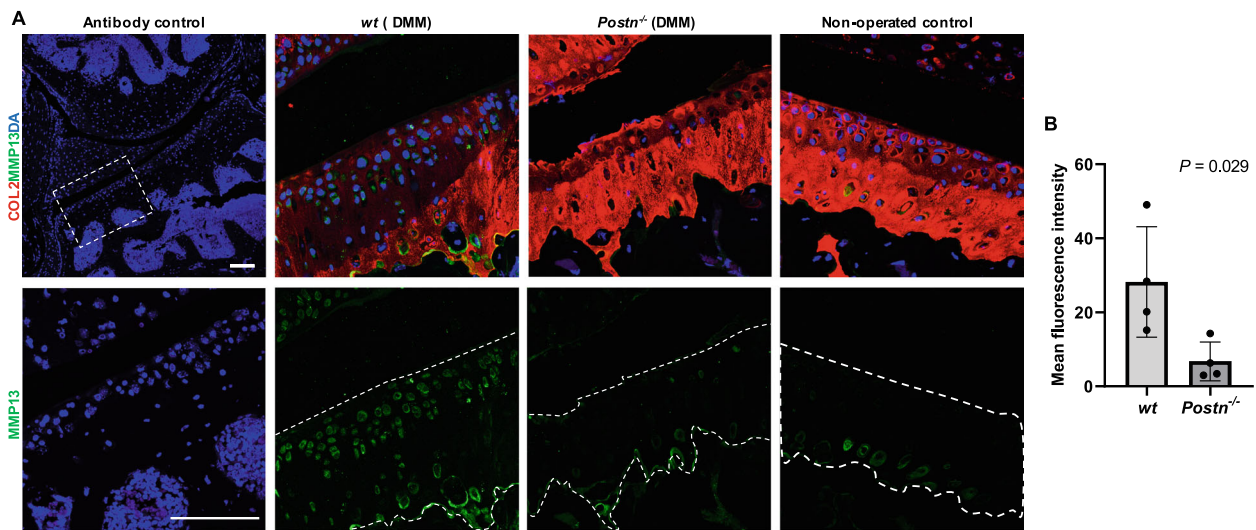


Fig. 4 *Postn*^{-/-} mice expressed less MMP-13 than *wt* mice after DMM. **a** Immunofluorescent analysis showed that MMP-13 staining (green) was higher in cartilage of DMM-operated limbs than in the non-operated control limb. *Postn*^{-/-} mice ($n = 4$) showed less staining of MMP-13 than *wt* mice ($n = 4$). Type II collagen (Col 2) (red) staining was used for location of cartilage. The dotted lines on lower panels indicate the Col 2-positive cartilage area based on the results in the upper panels. DAPI (blue) was used as a counterstain. Scale bars = 100 μ m. **b** Quantification of immunostaining intensity of MMP-13 showed that MMP-13 intensity was significantly lower in *Postn*^{-/-} mice ($n = 4$) than *wt* mice ($n = 4$). (Mann-Whitney test)

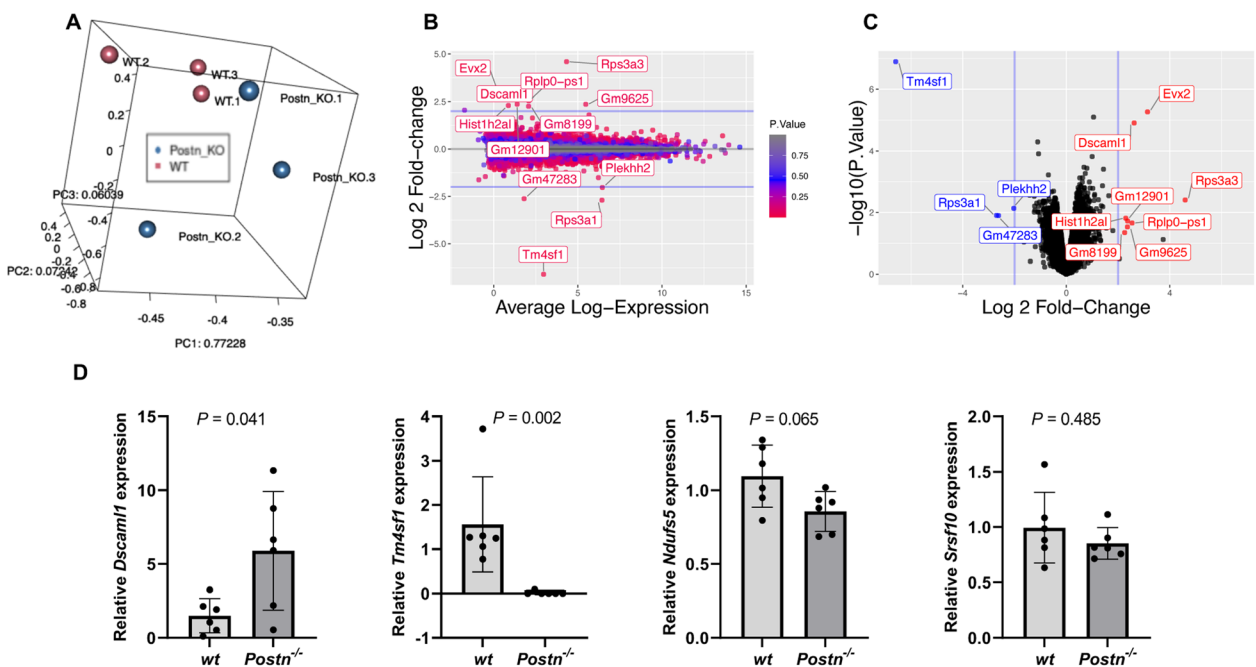


Fig. 5 Descriptive RNA-seq data and real-time PCR. **a** Principal component analysis of chondrocyte samples from *wt* ($n = 3$) and *Postn*^{-/-} ($n = 3$) mice showed distinct grouping based on gene expression differences. **b** MA (\log_2 ratio to mean expression) plot depicts expression fold change and averaged expression level of differentially expressed transcripts. **c** Volcano plot of all genes expressed greater than 1 count-per-million in all 6 samples where the observed \log_2 fold change is on the x -axis and the unadjusted P value converted to the $-\log_{10}$ scale is on the y -axis. Twelve genes with unadjusted $P \leq 0.05$ are highlighted in red when \log_2 fold changes $> +2$ and blue when < -2 . **d** Real-time PCR performed on chondrocytes isolated from an independent cohort of *wt* ($n = 6$) and *Postn*^{-/-} ($n = 6$) mice revealed an agreement with the RNA-seq data. (Mann-Whitney test)

wt mice than *Postn*^{-/-} mice. Moreover, we show that expression fold change and average expression levels vary subtly in a mean average (log₂ ratio to mean expression plot) (Fig. 5b).

Detection of differentially expressed gene transcripts

Gene transcripts (Supplemental Table 1) were significantly differentially expressed ($n = 1247$) between *Postn*^{-/-} and *wt* chondrocytes at an unadjusted $P \leq 0.05$ with 727 being upregulated in *Postn*^{-/-} while 520 were upregulated in *wt* chondrocytes. Out of 1247, only 48 transcripts had log₂ fold-change ≥ 2 . After, FDR ≤ 0.05 correction, only four transcripts (Table 4) were found to be differentially expressed (3 upregulated and 1 down-regulated) between *Postn*^{-/-} compared with *wt*. Volcano plot of genes expressed greater than 1 count-per-million in all six samples is shown (Fig. 5c).

Gene ontology annotation

Gene ontology analysis revealed that a number of distinct biological processes were significantly enriched for each genotype (Table 5). While the biological processes related to cell-cell adhesion, cell signaling, cell differentiation, focal adhesion, and angiogenesis were elevated in *Postn*^{-/-} mice, biological processes such as cell cycle, cell division, and DNA repair repressed in *Postn*^{-/-} mice.

Validation by real-time PCR

We further confirmed the differentially expressed genes by quantitative real-time PCR in agreement with the RNA-seq data (Fig. 5d).

Discussion

Our study illustrates that *Postn* deficiency exerts a protective effect against OA in mice. Specifically, mice lacking the *Postn* gene displayed significantly less cartilage degeneration than *wt* control mice in post-traumatic OA as well as age-related primary OA. *Postn* deficiency also appears to wield protective effects by modulating changes in the synovium and bone. Thus, our findings highlight that *Postn* loss-of-function protects against incidence and progression of OA independent of the cause, i.e., primary age-related spontaneous OA as well as injury-induced post-traumatic OA.

In both mouse models of OA, *Postn*^{-/-} mice retained superior cartilage and exhibited less degenerative

changes as measured by OARSI scores. These findings are consistent with the notion that protection from cartilage degeneration parallels protection from OA since cartilage degeneration is considered OA's hallmark [4]. Besides, we also showed that *Postn*^{-/-} mice developed significantly less synovitis than *wt* mice after DMM. Tajia et al. have also shown increased expression of *Postn* in human OA synovium [46]. These protective effects of *Postn* loss-of-function on the cartilage and synovium indicate decreased catabolic activity in the joint. Our observation aligns with our previous in vitro work showing that siRNA-mediated knockdown of *Postn* in chondrocytes results in reduced expression of inflammatory and catabolic markers such as IL-1 β , ADAMTS-4/5, and MMP-13 [12, 22].

We also found differences in trabecular bone parameters between the genotypes (*Postn*^{-/-} and *wt*) for both OA models. BV/TV, vBMD, Tb.Th, and Tb.N was low and Tb. Sp was high in *Postn*^{-/-} mice. These parameters are not only standard osteoporosis measurements but have also been used as markers for OA [47–49]. The pattern of these bony changes in *Postn*^{-/-} mice mirrors OA protection as has been noted in rodent and human studies of OA [31, 47–52]. These findings suggest that *Postn* plays a role in modulating changes in cartilage as well as in the bone. However, it is not possible to conclude that the bone is driving the cartilage phenotype from this investigation.

In the present study, we did not examine how the genetic deficiency of *Postn* protects mice from developing OA. However, several studies suggest a possible link connecting the mechanisms of *Postn*-mediated cartilage degeneration with NF- κ B and Wnt signaling [7, 12, 22, 53]. We have previously shown that *Postn* expression is increased following injury [12]. *Postn* is upregulated in human OA cartilage and cartilage from mice undergoing DMM and is correlated with increased MMP-13 expression in OA cartilage [12, 22]. Increased expression of *Postn* leads to overexpression of cartilage ECM degrading enzymes such as MMP-13 and ADAMTS-5. *Postn* also promotes condylar resorption via the NF- κ B-ADAMTS-5 axis in temporomandibular joint OA [54]. Overexpression of *Postn* by the administration of recombinant proteins or through lentivirus transduction leads to increased expression of MMP-13 in human and murine chondrocytes. Likewise, *Postn* inhibition or

Table 4 Gene transcripts differentially expressed in chondrocytes between *Postn*^{-/-} and *wt* mice

Gene symbol	Gene name	Log ₂ fold change	P	Description
<i>Evx2</i>	Even skipped homeobox 2	3.14	5.30×10^{-6}	Up-regulated in <i>Postn</i> ^{-/-} mice
<i>Dscaml1</i>	DS cell adhesion molecule like 1	2.62	1.22×10^{-5}	Up-regulated in <i>Postn</i> ^{-/-} mice
<i>Gdf10</i>	Growth differentiation factor 10	1.05	7.85×10^{-6}	Up-regulated in <i>Postn</i> ^{-/-} mice
<i>Tm4sf1</i>	Transmembrane 4 superfamily member 1	-6.59	1.27×10^{-7}	Down-regulated in <i>Postn</i> ^{-/-} mice

Table 5 Biological processes (gene ontologies) altered in chondrocytes between *Postn*^{-/-} and *wt* mice

Gene ontology term (elevated in <i>Postn</i> ^{-/-} mice)	Log ₂ fold change	FDR	Gene ontology term (repressed in <i>Postn</i> ^{-/-} mice)	Log ₂ fold change	FDR
Cell-cell adhesion	4.60	1.44 × 10 ⁻³	Mitotic cell cycle process	-7.75	2.99 × 10 ⁻¹¹
Regulation of developmental process	4.70	1.09 × 10 ⁻³	Mitotic nuclear division	-6.77	1.64 × 10 ⁻⁸
Regulation of response to stimulus	5.06	3.01 × 10 ⁻⁴	Cell division	-7.39	3.16 × 10 ⁻¹⁰
Blood vessel morphogenesis	4.52	1.89 × 10 ⁻³	Chromosome organization	-7.06	1.30 × 10 ⁻⁹
Cell differentiation	4.62	1.34 × 10 ⁻³	Chromosome segregation	-8.17	1.25 × 10 ⁻¹¹
Regulation of signaling	5.53	4.01 × 10 ⁻⁵	Cell cycle	-7.29	3.49 × 10 ⁻¹⁰
Biological adhesion	5.75	2.10 × 10 ⁻⁵	DNA repair	-7.79	2.99 × 10 ⁻¹¹
Regulation of cell communication	5.53	4.01 × 10 ⁻⁵	DNA-dependent DNA replication	-6.61	8.23 × 10 ⁻⁸
Regulation of signal transduction	5.38	7.68 × 10 ⁻⁵	DNA replication	-6.36	1.51 × 10 ⁻⁷
Angiogenesis	4.47	2.03 × 10 ⁻³	Double-strand break repair	-5.85	4.04 × 10 ⁻⁶

FDR false discovery rate

deficiency results in decreased expression of catabolic enzymes. Therefore, we surmise that loss of *Postn* protects against cartilage degeneration by decreasing ECM degrading enzymes such as MMP-13 and ADAMTS-5. A recent study identified DDR-1 as a potential receptor for *Postn*-mediated signaling in chondrocytes. It showed that blocking DDR-1 with small chemical inhibitors reduced MMP-13 expression and cartilage degradation in vitro and in vivo [53].

Baseline transcriptomic differences between *Postn*^{-/-} and *wt* mice revealed interesting findings. The expression of *Evx2*, *Dscaml1*, and *Gdf10* increased in *Postn*^{-/-} compared with *wt* mice. *Evx2* is predominantly expressed in the limbs and is involved in vertebrate limbs' morphogenesis, where it interacts with Hox genes [55]. *Dscaml1* is a member of the immunoglobulin superfamily of cell adhesion molecules, which participates in neuronal differentiation [56]. Tuure et al. reported that the expression of *Dscaml1* is low in human OA chondrocytes treated with IL-1 β and is increased following treatment with a selective inhibitor of microsomal prostaglandin E synthase 1 [57]. *Gdf10* gene encodes a secreted ligand of transforming growth factor-beta superfamily of proteins, which plays essential functions in chondrocyte differentiation and bone formation [58]. In particular, it was found that the expression of *Gdf10* was increased in chondrocytes under hypoxia, where *Gdf10* was regulated by Sox-9, suggesting its protective role in chondrocytes [59]. The expression of *Tm4sf1* was decreased in *Postn*^{-/-} mice. *Tm4sf1* is a surface marker, known to inhibit apoptosis and promote cell proliferation and migration [60]. This transcriptomic profile paralleled with gene ontology annotations. For instance, the biological processes related to cell-cell adhesion, cell signaling, cell differentiation, and focal adhesion were elevated in *Postn*^{-/-} mice, while biological

processes such as cell cycle, cell division, and proliferation were repressed in *Postn*^{-/-} mice. Together, these findings provide novel insights into the role of *Postn* in chondrocytes, specifically highlighting that increased expression of *Dscaml1* and *Gdf10* (and related biological processes) offers protection from OA, while the expression of *Tm4sf1* (and related biological processes) related to cellular phenotypes that are altered with *Postn* knockout. While the role of *Postn* in OA has been discussed in the previous paragraph, here, we highlight its role in cell functions. Chinzei et al. showed that exogenous overexpression of *Postn* increases chondrocyte migration which is impeded by its knockdown [22]. Likewise, Padiál-Molina et al. reported an increase in proliferation and migration of periodontal ligament fibroblasts with *Postn* treatment [61]. Finally, Cai and colleagues showed that *Postn* knockdown decreases cell matrix [23]; however, no data are yet available for cell-cell-adhesion in the context of *Postn* knockdown or overexpression in chondrocytes.

Our finding that *Postn* deficiency reduces both age-related spontaneous OA and post-traumatic OA is important. While aging and obesity are associated with primary idiopathic OA [62–65], joint injuries cause post-traumatic OA cases [66, 67] and constitute at least 12% of OA [68]. While both OA forms are qualitatively similar in that both share standard features such as cartilage degeneration and bone sclerosis [69], the underlying disease mechanisms are dissimilar in many ways [10]. However, their degree of overlap is unclear, particularly at the mechanistic level. Our finding that *Postn* deficiency protected the joint from cartilage degeneration and bone alterations in both types of OA suggests that *Postn* ablation may have widely applicable therapeutic efficacy. Specifically, anti-*Postn* therapy may have utility for primary idiopathic OA as well as for post-traumatic OA.

In this study, we have shown that global deletion of *Postn* is protective against OA. *Postn* knockout is embryonically non-lethal, yet some *Postn*^{-/-} mice die shortly after birth. Surviving mice have 10–20% growth retardation and exhibit some skeletal abnormalities such as shorter subchondral bone, weaker ligaments, and moderate scoliosis (Cai et al. unpublished data), which complicate mechanistic exploration in a specific tissue, cartilage, for example. Thus, in future studies, we will disable *Postn* in a temporal (inducible) and cartilage-specific manner by genetic ablation in mature mice to study OA development.

This study has some limitations, we did not report data from heterozygotes (*Postn*^{+/-}) since no protective effect was observed in those mice. Other limitations included the lack of measurement of functional outcomes such as behavior, pain, and gait as well as the lack of assessment of progressive changes as the only one-time point was studied in both models. Moreover, detailed analysis of osteophyte structure and histology is lacking. Another limiting factor was also difficulty to breed and raise *Postn* homozygous mice due to post-natal death of mice. Due to limiting number of mice available “sham” procedure could not be performed and could be a superior control for this model. Lastly, as we performed bulk RNA-seq only on primary chondrocytes, the findings should be interpreted within the context of cartilage. Since OA is considered a whole-joint disease and *Postn* plays a role in the bone and probably other parts of the joint, the lack of data from other tissue and cell types is a limitation.

Conclusions

In summary, *Postn* genetic loss-of-function protects against DMM-induced post-traumatic and age-related spontaneous OA. Our data identify *Postn* as a novel therapeutic target to delay or prevent OA, independent of the cause despite aforementioned limitations. Further mechanistic studies are warranted to investigate the tissue-specific role(s) of *Postn* in OA and its impact on other knee tissues such as meniscus and ligaments. *Postn* modulating therapies will have to be identified and tested before these findings have translational value in the clinical setting.

Abbreviations

Postn: Periostin; OA: Osteoarthritis; wt: Wild type; DMM: Destabilization of the medial meniscus; MMP-13: Matrix metalloproteinase 13 (collagenase 3); PCR: Polymerase chain reaction; ELISA: Enzyme-linked immunosorbent assay; OARS: Osteoarthritis Research Society International; μ CT: Micro-computed tomography; PBS: Phosphate-buffered saline; NGS: Normal goat serum; COL-2: Collagen type II; DAPI: 4', 6-Diamidino-2-phenylindole; BV/TV: Bone volume fraction; vBMD: Volumetric bone mineral density; Tb.Th: Trabecular thickness; Tb.N: Trabecular number; Tb.Sp: Trabecular spacing; FBS: Fetal bovine serum; DMEM: Dulbecco's modified Eagle's medium; RIN: RNA integrity number; FDR: False-discovery rate; GO: Gene ontology; CI: Confidence interval; ECM: Extracellular matrix; *Evx2*: Even skipped home box 2; *Dscam1l*: DS cell adhesion molecule like one; *Gdf10*: Growth differentiation factor 10; *Tm4sf1*: Transmembrane four superfamily member 1; *Ndufs5*: NADH:ubiquinone oxidoreductase core subunit 55; *Srsf10*: Serine/arginine-rich splicing factor 10; *Gapdh*: Glyceraldehyde-3-phosphate

dehydrogenase; ADAMTS: A disintegrin and metalloproteinase with thrombospondin motif; NF- κ B: Nuclear factor kappa-light-chain-enhancer of activated B cells; DDR-1: Discoidin domain receptor 1; IL-1 β : Interleukin 1 beta; Sox-9: SRY (sex-determining region Y) box transcription factor 9; DAB: 3,3'-Diaminobenzidine

Supplementary Information

The online version contains supplementary material available at <https://doi.org/10.1186/s13075-021-02477-z>.

Additional file 1. Gene transcripts

Acknowledgements

The authors sincerely thank the critical technical assistance provided by Crystal Idleburg and Samantha Coleman from Histology & Morphometry Core of the Musculoskeletal Research Center (NIAMS/NIH P30 AR074992, PI: Silva) at Washington University, St. Louis, MO. The authors much appreciate the support provided by the New York University μ CT services (S10 OD010751). The authors also thank the Genome Technology Access Center at Washington University School of Medicine for RNA-seq analysis. The center is partially supported by NCI Cancer Center Support Grant P30 CA91842 to the Siteman Cancer Center and by ICTS/CTSA Grant UL1TR002345 from the NCR, a component of the NIH and NIH Roadmap for Medical Research. This publication is solely the authors' responsibility and does not necessarily represent the official view of NIAMS, NCR, or NIH.

Authors' contributions

All authors were involved in drafting the article or revising it critically for important intellectual content, and all authors approved the final version to be published. Drs. Attur and Rai had full access to all the data in the study and take responsibility for the integrity of the data and accuracy of the data analysis. Study conception and design. Mukundan Attur, Xin Duan, Lei Cai, Weili Zhang, Eric D. Tycksen, Robert H. Brophy, Steven Abramson and Muhammad Farooq Rai. Analysis and interpretation of data. Mukundan Attur, Xin Duan, Lei Cai, Tianzhen Han, Weili Zhang, Eric D. Tycksen, Robert H. Brophy, Steven Abramson, and Muhammad Farooq Rai.

Author information

Mukundan Attur and Xin Duan contributed equally to this work.

Funding

This study was supported by research funding by the Department of Orthopedic Surgery, Washington University School of Medicine, St. Louis, MO. Dr. Rai is also supported through the Pathway to Independence Award (R00 AR064837) from the National Institute of Arthritis and Musculoskeletal and Skin Diseases (NIAMS), National Institutes of Health (NIH). The study was also supported by the NIAMS (NIH) R01 AR052873 and R01 AR054817 to Dr. Abramson. The content of this publication is solely the responsibility of the authors and does not necessarily represent the official views of the NIH or NIAMS.

Availability of data and materials

RNA-seq data have been deposited to the GEO and are accessible through the accession number GSE164534 at <https://www.ncbi.nlm.nih.gov/geo/>. The other datasets generated and/or analyzed during the current study are not publicly available due to the limit of storage space but are available from the corresponding authors on a reasonable request.

Declarations

Ethics approval and consent to participate

All the animal studies were carried out in accordance with the recommendations in the Guide for the Care and Use of Laboratory Animals of the National Institutes of Health. All procedures were approved by the Institutional Animal Care and Use Committee (IACUC) of Washington University School of Medicine (Protocol No. 20190113) and New York University Grossman School of Medicine (Protocol No. s16-00601).

Consent for publication

Not applicable

Competing interests

The authors declare that they have no competing interests.

Author details

¹Division of Rheumatology, Department of Medicine, New York University Grossman School of Medicine, Langone Orthopedic Hospital, 550 1st Avenue, New York, NY 10016, USA. ²Department of Orthopaedic Surgery, Washington University School of Medicine at Barnes-Jewish Hospital MS 8233, 425 South Euclid Avenue, St. Louis, MO 63110, USA. ³Present address: Bluestone Center for Clinical Research, NYU College of Dentistry, New York, NY 10010, USA. ⁴Genome Technology Access Center, McDonnell Genome Institute, Washington University School of Medicine, St. Louis 63110, MO, USA. ⁵Department of Cell Biology & Physiology, Washington University School of Medicine, St. Louis 63110, MO, USA.

Received: 26 January 2021 Accepted: 10 March 2021

Published online: 08 April 2021

References

- Kotlarz H, Gunnarsson CL, Fang H, Rizzo JA. Insurer and out-of-pocket costs of osteoarthritis in the US: evidence from national survey data. *Arthritis Rheum.* 2009;60(12):3546–53. <https://doi.org/10.1002/art.24984>.
- Pereira D, Peleteiro B, Araujo J, Branco J, Santos RA, Ramos E. The effect of osteoarthritis definition on prevalence and incidence estimates: a systematic review. *Osteoarthr Cartil.* 2011;19(11):1270–85. <https://doi.org/10.1016/j.joca.2011.08.009>.
- Poole AR. Osteoarthritis as a whole joint disease. *HSS J.* 2012;8(1):4–6. <https://doi.org/10.1007/s11420-011-9248-6>.
- Loeser RF, Goldring SR, Scanzello CR, Goldring MB. Osteoarthritis: a disease of the joint as an organ. *Arthritis Rheum.* 2012;64(6):1697–707. <https://doi.org/10.1002/art.34453>.
- Poulet B. Models to define the stages of articular cartilage degradation in osteoarthritis development. *Int J Exp Pathol.* 2017;98(3):120–6. <https://doi.org/10.1111/iep.12230>.
- Lourido L, Calamia V, Mateos J, Fernandez-Puente P, Fernandez-Tajes J, Blanco FJ, Ruiz-Romero C. Quantitative proteomic profiling of human articular cartilage degradation in osteoarthritis. *J Proteome Res.* 2014;13(12):6096–106. <https://doi.org/10.1021/pr501024p>.
- Chijimatsu R, Kunugiza Y, Taniyama Y, Nakamura N, Tomita T, Yoshikawa H. Expression and pathological effects of periostin in human osteoarthritis cartilage. *BMC Musculoskelet Disord.* 2015;16(1):215. <https://doi.org/10.1186/s12891-015-0682-3>.
- Rousseau JC, Sornay-Rendu E, Bertholon C, Garnero P, Chapurlat R. Serum periostin is associated with prevalent knee osteoarthritis and disease incidence/progression in women: the OFELY study. *Osteoarthr Cartil.* 2015; 23(10):1736–42. <https://doi.org/10.1016/j.joca.2015.05.015>.
- Honsawek S, Wilairatana V, Udomsinprasert W, Sinlapavilawan P, Jirathanathornnukul N. Association of plasma and synovial fluid periostin with radiographic knee osteoarthritis: cross-sectional study. *Joint Bone Spine.* 2015;82(5):352–5. <https://doi.org/10.1016/j.jbspin.2015.01.023>.
- Loeser RF, Olex AL, McNulty MA, Carlson CS, Callahan MF, Ferguson CM, Chou J, Leng X, Fetrow JS. Microarray analysis reveals age-related differences in gene expression during the development of osteoarthritis in mice. *Arthritis Rheum.* 2012;64(3):705–17. <https://doi.org/10.1002/art.33388>.
- Chou CH, Wu CC, Song JW, Chuang HP, Lu LS, Chang JH, Kuo SY, Lee CH, Wu JY, Chen YT, Kraus V, Lee MTM. Genome-wide expression profiles of subchondral bone in osteoarthritis. *Arthritis Res Ther.* 2013;15(6):R190. <https://doi.org/10.1186/ar4380>.
- Attur M, Yang Q, Shimada K, Tachida Y, Nagase H, Mignatti P, Statman L, Palmer G, Kirsch T, Beier F, Abramson SB. Elevated expression of periostin in human osteoarthritic cartilage and its potential role in matrix degradation via matrix metalloproteinase-13. *FASEB J.* 2015;29(10):4107–21. <https://doi.org/10.1096/fj.15-272427>.
- Coutu DL, Wu JH, Monette A, Rivard GE, Blostein MD, Galipeau J. Periostin, a member of a novel family of vitamin K-dependent proteins, is expressed by mesenchymal stromal cells. *J Biol Chem.* 2008;283(26):17991–8001. <https://doi.org/10.1074/jbc.M708029200>.
- Takehita S, Kikuno R, Tezuka K, Amann E. Osteoblast-specific factor 2: cloning of a putative bone adhesion protein with homology with the insect protein fasciclin I. *Biochem J.* 1993;294(Pt 1):271–8. <https://doi.org/10.1042/bj2940271>.
- Horiuchi K, Amizuka N, Takehita S, Takamatsu H, Katsuura M, Ozawa H, Toyama Y, Bonewald LF, Kudo A. Identification and characterization of a novel protein, periostin, with restricted expression to periosteum and periodontal ligament and increased expression by transforming growth factor beta. *J Bone Miner Res.* 1999;14(7):1239–49. <https://doi.org/10.1359/jbmr.1999.14.7.1239>.
- Conway SJ, Izuhara K, Kudo Y, Litvin J, Markwald R, Ouyang G, Arron JR, Holweg CT, Kudo A. The role of periostin in tissue remodeling across health and disease. *Cell Mol Life Sci.* 2014;71(7):1279–88. <https://doi.org/10.1007/s00018-013-1494-y>.
- Litvin J, Selim AH, Montgomery MO, Lehmann K, Rico MC, Devlin H, Bednarik DP, Safadi FF. Expression and function of periostin-isoforms in bone. *J Cell Biochem.* 2004;92(5):1044–61. <https://doi.org/10.1002/jcb.20115>.
- Zhu S, Barbe MF, Amin N, Rani S, Popoff SN, Safadi FF, Litvin J. Immunolocalization of Periostin-like factor and Periostin during embryogenesis. *J Histochem Cytochem.* 2008;56(4):329–45. <https://doi.org/10.1369/jhc.7A7321.2007>.
- Ma D, Zhang R, Sun Y, Rios HF, Haruyama N, Han X, Kulkarni AB, Qin C, Feng JQ. A novel role of periostin in postnatal tooth formation and mineralization. *J Biol Chem.* 2011;286(6):4302–9. <https://doi.org/10.1074/jbc.M110.140202>.
- Norris RA, Damon B, Mironov V, Kasyanov V, Ramamurthi A, Moreno-Rodriguez R, Trusk T, Potts JD, Goodwin RL, Davis J, Hoffman S, Wen X, Sugi Y, Kern CB, Mjaatvedt CH, Turner DK, Oka T, Conway SJ, Molkentin JD, Forgacs G, Markwald RR. Periostin regulates collagen fibrillogenesis and the biomechanical properties of connective tissues. *J Cell Biochem.* 2007;101(3):695–711. <https://doi.org/10.1002/jcb.21224>.
- Hamilton DW. Functional role of periostin in development and wound repair: implications for connective tissue disease. *J Cell Commun Signal.* 2008;2(1–2):9–17. <https://doi.org/10.1007/s12079-008-0023-5>.
- Chinzei N, Brophy RH, Duan X, Cai L, Nunley RM, Sandell LJ, Rai MF. Molecular influence of anterior cruciate ligament tear remnants on chondrocytes: a biologic connection between injury and osteoarthritis. *Osteoarthr Cartil.* 2018; 26(4):588–99. <https://doi.org/10.1016/j.joca.2018.01.017>.
- Cai L, Brophy RH, Tycksen ED, Duan X, Nunley RM, Rai MF. Distinct expression pattern of periostin splice variants in chondrocytes and ligament progenitor cells. *FASEB J.* 2019;33(7):8386–405. <https://doi.org/10.1096/fj.201802281R>.
- Bonnet N, Gineyts E, Ammann P, Conway SJ, Garnero P, Ferrari S. Periostin deficiency increases bone damage and impairs injury response to fatigue loading in adult mice. *PLoS One.* 2013;8(10):e78347. <https://doi.org/10.1371/journal.pone.0078347>.
- Duchamp de Lageneste O, Julien A, Abou-Khalil R, Frangi G, Carvalho C, Cagnard N, Cordier C, Conway SJ, Colnot C. Periosteum contains skeletal stem cells with high bone regenerative potential controlled by Periostin. *Nat Commun.* 2018;9(1):773.
- Yu L, Wang J, Liu K. Role of periostin in ECRS. *Eur Arch Otorhinolaryngol.* 2020. <https://doi.org/10.1007/s00405-020-06369-x>.
- Nakazeki F, Nishiga M, Horie T, Nishi H, Nakashima Y, Baba O, Kuwabara Y, Nishino T, Nakao T, Ide Y, Koyama S, Kimura M, Tsuji S, Sowa N, Yoshida S, Conway SJ, Yanagita M, Kimura T, Ono K. Loss of periostin ameliorates adipose tissue inflammation and fibrosis in vivo. *Sci Rep.* 2018;8(11):8553. <https://doi.org/10.1038/s41598-018-27009-9>.
- Idolazzi L, Ridolo E, Fassio A, Gatti D, Montagni M, Caminati M, Martignago I, Incorvaia C, Senna G. Periostin: the bone and beyond. *Eur J Intern Med.* 2017;38:12–6. <https://doi.org/10.1016/j.ijem.2016.11.015>.
- Ma HL, Blanchet TJ, Peluso D, Hopkins B, Morris EA, Glasson SS. Osteoarthritis severity is sex dependent in a surgical mouse model. *Osteoarthr Cartil.* 2007; 15(6):695–700. <https://doi.org/10.1016/j.joca.2006.11.005>.
- Glasson SS, Blanchet TJ, Morris EA. The surgical destabilization of the medial meniscus (DMM) model of osteoarthritis in the 129/SvEv mouse. *Osteoarthr Cartil.* 2007;15(9):1061–9. <https://doi.org/10.1016/j.joca.2007.03.006>.
- Chinzei N, Rai MF, Hashimoto S, Schmidt EJ, Takebe K, Cheverud JM, Sandell LJ. Evidence for genetic contribution to variation in posttraumatic osteoarthritis in mice. *Arthritis Rheumatol.* 2019;71(3):370–81. <https://doi.org/10.1002/art.40730>.
- Glasson SS, Chambers MG, Van Den Berg WB, Little CB. The OARSI histopathology initiative - recommendations for histological assessments of

- osteoarthritis in the mouse. *Osteoarthr Cartil.* 2010;18(Suppl 3):S17–23. <https://doi.org/10.1016/j.joca.2010.05.025>.
33. Lewis JS, Hembree WC, Furman BD, Tippets L, Cattel D, Huebner JL, Little D, DeFrate LE, Kraus VB, Guilak F, et al. Acute joint pathology and synovial inflammation is associated with increased intra-articular fracture severity in the mouse knee. *Osteoarthr Cartil.* 2011;19(7):864–73. <https://doi.org/10.1016/j.joca.2011.04.011>.
 34. Takebe K, Rai MF, Schmidt EJ, Sandell LJ. The chemokine receptor CCR5 plays a role in post-traumatic cartilage loss in mice, but does not affect synovium and bone. *Osteoarthr Cartil.* 2015;23(3):454–61. <https://doi.org/10.1016/j.joca.2014.12.002>.
 35. Dempster DW, Compston JE, Drezner MK, Glorieux FH, Kanis JA, Malluche H, Meunier PJ, Ott SM, Recker RR, Parfitt AM. Standardized nomenclature, symbols, and units for bone histomorphometry: a 2012 update of the report of the ASBMR Histomorphometry Nomenclature Committee. *J Bone Miner Res.* 2013;28(1):2–17. <https://doi.org/10.1002/jbmr.1805>.
 36. Duan X, Cai L, Schmidt EJ, Shen J, Tycksen ED, O'Keefe RJ, Cheverud JM, Rai MF. RNA-seq analysis of chondrocyte transcriptome reveals genetic heterogeneity in LG/J and SM/J murine strains. *Osteoarthr Cartil.* 2020;28(4):516–27. <https://doi.org/10.1016/j.joca.2020.01.001>.
 37. Dobin A, Davis CA, Schlesinger F, Drenkow J, Zaleski C, Jha S, Batut P, Chaisson M, Gingeras TR. STAR: ultrafast universal RNA-seq aligner. *Bioinformatics.* 2013;29(1):15–21. <https://doi.org/10.1093/bioinformatics/bts635>.
 38. Liao Y, Smyth GK, Shi W. featureCounts: an efficient general purpose program for assigning sequence reads to genomic features. *Bioinformatics.* 2014;30(7):923–30. <https://doi.org/10.1093/bioinformatics/btt656>.
 39. Wang L, Wang S, Li W. RSeQC: quality control of RNA-seq experiments. *Bioinformatics.* 2012;28(16):2184–5. <https://doi.org/10.1093/bioinformatics/bts356>.
 40. Robinson MD, McCarthy DJ, Smyth GK. edgeR: a bioconductor package for differential expression analysis of digital gene expression data. *Bioinformatics.* 2010;26(1):139–40. <https://doi.org/10.1093/bioinformatics/btp616>.
 41. Ritchie ME, Phipson B, Wu D, Hu Y, Law CW, Shi W, Smyth GK. limma powers differential expression analyses for RNA-sequencing and microarray studies. *Nucleic Acids Res.* 2015;43(7):e47. <https://doi.org/10.1093/nar/gkv007>.
 42. Liu R, Holik AZ, Su S, Jansz N, Chen K, Leong HS, Blewitt ME, Asselin-Labat ML, Smyth GK, Ritchie ME. Why weight? Modelling sample and observational level variability improves power in RNA-seq analyses. *Nucleic Acids Res.* 2015;43(15):e97. <https://doi.org/10.1093/nar/gkv412>.
 43. Leek JT, Johnson WE, Parker HS, Jaffe AE, Storey JD. The sva package for removing batch effects and other unwanted variation in high-throughput experiments. *Bioinformatics.* 2012;28(6):882–3. <https://doi.org/10.1093/bioinformatics/bts034>.
 44. Luo W, Friedman MS, Shedden K, Hankenson KD, Woolf PJ. GAGE: generally applicable gene set enrichment for pathway analysis. *BMC Bioinformatics.* 2009;10(1):161. <https://doi.org/10.1186/1471-2105-10-161>.
 45. Zhao S, Guo Y, Sheng Q, Shyr Y. Advanced heat map and clustering analysis using heatmap3. *Biomed Res Int.* 2014;2014:986048.
 46. Tajika Y, Moue T, Ishikawa S, Asano K, Okumo T, Takagi H, Hisamitsu T. Influence of periostin on synoviocytes in knee osteoarthritis. *In Vivo.* 2017;31(1):69–77. <https://doi.org/10.21873/invivo.11027>.
 47. Lee JH, Chun KJ, Kim HS, Kim SH, Han P, Jun Y, Lim D. Alteration patterns of trabecular bone microarchitectural characteristics induced by osteoarthritis over time. *Clin Interv Aging.* 2012;7:303–12.
 48. Patel V, Isever AS, Burghardt A, Laib A, Ries M, Majumdar S. MicroCT evaluation of normal and osteoarthritic bone structure in human knee specimens. *J Orthop Res.* 2003;21(1):6–13. [https://doi.org/10.1016/S0736-0266\(02\)00093-1](https://doi.org/10.1016/S0736-0266(02)00093-1).
 49. Fang H, Huang L, Welch I, Norley C, Holdsworth DW, Beier F, Cai D. Early changes of articular cartilage and subchondral bone in the DMM mouse model of osteoarthritis. *Sci Rep.* 2018;8(1):2855. <https://doi.org/10.1038/s41598-018-21184-5>.
 50. Hashimoto S, Rai MF, Janiszak KL, Cheverud JM, Sandell LJ. Cartilage and bone changes during development of post-traumatic osteoarthritis in selected LGXSM recombinant inbred mice. *Osteoarthr Cartil.* 2012;20(6):562–71. <https://doi.org/10.1016/j.joca.2012.01.022>.
 51. Rai MF, Duan X, Quirk JD, Holguin N, Schmidt EJ, Chinzei N, Silva MJ, Sandell LJ. Post-traumatic osteoarthritis in mice following mechanical injury to the synovial joint. *Sci Rep.* 2017;7(1):45223. <https://doi.org/10.1038/srep45223>.
 52. Glasson SS, Askew R, Sheppard B, Carito B, Blanchet T, Ma HL, Flannery CR, Peluso D, Kanki K, Yang Z, Majumdar MK, Morris EA. Deletion of active ADAMTS5 prevents cartilage degradation in a murine model of osteoarthritis. *Nature.* 2005;434(7033):644–8. <https://doi.org/10.1038/nature03369>.
 53. Han T, Mignatti P, Abramson SB, Attur M. Periostin interaction with discoidin domain receptor-1 (DDR1) promotes cartilage degeneration. *PLoS One.* 2020;15(4):e0231501. <https://doi.org/10.1371/journal.pone.0231501>.
 54. Fan B, Liu X, Chen X, Xu W, Zhao H, Yang C, Zhang S. Periostin mediates condylar resorption via the NF-kappaB-ADAMTS5 pathway. *Inflammation.* 2020;43(2):455–65. <https://doi.org/10.1007/s10753-019-01129-4>.
 55. Herault Y, Hraba-Renevey S, van der Hoeven F, Douboué D. Function of the *Evx-2* gene in the morphogenesis of vertebrate limbs. *EMBO J.* 1996;15(23):6727–38. <https://doi.org/10.1002/j.1460-2075.1996.tb01062.x>.
 56. Agarwala KL, Ganesh S, Tsutsumi Y, Suzuki T, Amano K, Yamakawa K. Cloning and functional characterization of DSCAML1, a novel DSCAM-like cell adhesion molecule that mediates homophilic intercellular adhesion. *Biochem Biophys Res Commun.* 2001;285(3):760–72. <https://doi.org/10.1006/bbrc.2001.5214>.
 57. Tuure L, Pemmari A, Hamalainen M, Moilanen T, Moilanen E. Regulation of gene expression by MF63, a selective inhibitor of microsomal PGE synthase 1 (mPGES1) in human osteoarthritic chondrocytes. *Br J Pharmacol.* 2020;177(18):4134–46. <https://doi.org/10.1111/bph.15142>.
 58. Kaihara S, Bessho K, Okubo Y, Sonobe J, Komatsu Y, Miura M, Miyatake S, Nakao K, Iizuka T. Over expression of bone morphogenetic protein-3b (BMP-3b) using an adenoviral vector promote the osteoblastic differentiation in C2C12 cells and augment the bone formation induced by bone morphogenetic protein-2 (BMP-2) in rats. *Life Sci.* 2003;72(15):1683–93. [https://doi.org/10.1016/S0024-3205\(02\)02477-3](https://doi.org/10.1016/S0024-3205(02)02477-3).
 59. Lafont JE, Talma S, Hopfgarten C, Murphy CL. Hypoxia promotes the differentiated human articular chondrocyte phenotype through SOX9-dependent and -independent pathways. *J Biol Chem.* 2008;283(8):4778–86. <https://doi.org/10.1074/jbc.M707729200>.
 60. Wei Y, Shen X, Li L, Cao G, Cai X, Wang Y, Shen H. TM45F1 inhibits apoptosis and promotes proliferation, migration and invasion in human gastric cancer cells. *Oncol Lett.* 2018;16(5):6081–8. <https://doi.org/10.3892/ol.2018.9411>.
 61. Padiál-Molina M, Volk SL, Rios HF. Periostin increases migration and proliferation of human periodontal ligament fibroblasts challenged by tumor necrosis factor -alpha and Porphyromonas gingivalis lipopolysaccharides. *J Periodontol Res.* 2014;49(3):405–14. <https://doi.org/10.1111/jre.12120>.
 62. Loeser RF. Aging and osteoarthritis. *Curr Opin Rheumatol.* 2011;23(5):492–6. <https://doi.org/10.1097/BOR.0b013e3283494005>.
 63. Rai MF, Sandell LJ. Inflammatory mediators: tracing links between obesity and osteoarthritis. *Crit Rev Eukaryot Gene Expr.* 2011;21(2):131–42. <https://doi.org/10.1615/CritRevEukaryotGeneExpr.v21.i2.30>.
 64. Loeser RF. Aging and osteoarthritis: the role of chondrocyte senescence and aging changes in the cartilage matrix. *Osteoarthr Cartil.* 2009;17(8):971–9. <https://doi.org/10.1016/j.joca.2009.03.002>.
 65. Griffin TM, Guilak F. Why is obesity associated with osteoarthritis? Insights from mouse models of obesity. *Biorheology.* 2008;45(3–4):387–98. <https://doi.org/10.3233/BIR-2008-0485>.
 66. Thomas AC, Hubbard-Turner T, Wikstrom EA, Palmieri-Smith RM. Epidemiology of posttraumatic osteoarthritis. *J Athl Train.* 2017;52(6):491–6. <https://doi.org/10.4085/1062-6050-51.5.08>.
 67. Punzi L, Galozzi P, Luisetto R, Favero M, Ramonda R, Oliviero F, Scanu A. Post-traumatic arthritis: overview on pathogenic mechanisms and role of inflammation. *RMD Open.* 2016;2(2):e000279. <https://doi.org/10.1136/rmdopen-2016-000279>.
 68. Brown TD, Johnston RC, Saltzman CL, Marsh JL, Buckwalter JA. Posttraumatic osteoarthritis: a first estimate of incidence, prevalence, and burden of disease. *J Orthop Trauma.* 2006;20(10):739–44. <https://doi.org/10.1097/01.bot.0000246468.80635.ef>.
 69. McNulty MA, Loeser RF, Davey C, Callahan MF, Ferguson CM, Carlson CS. Histopathology of naturally occurring and surgically induced osteoarthritis in mice. *Osteoarthr Cartil.* 2012;20(8):949–56. <https://doi.org/10.1016/j.joca.2012.05.001>.

Publisher's Note

Springer Nature remains neutral with regard to jurisdictional claims in published maps and institutional affiliations.